Food Chemistry: X 18 (2023) 100734

Contents lists available at ScienceDirect

Food Chemistry: X

journal homepage: www.sciencedirect.com/journal/food-chemistry-x

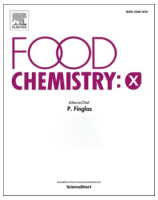

Probing the mechanism of interaction between capsaicin and myofibrillar proteins through multispectral, molecular docking, and molecular dynamics simulation methods

Zhicheng Wu [a], Jingbing Xu [d], Jinggang Ruan [a], Jiaxin Chen [a,b], Xue Li [e], Yiru Yu [a], Xinrui Xie [a], Jie Tang [a,b,*], Dong Zhang [a,b,c,*], Hongjun Li [f]

[a] College of Food and Bioengineering, Xihua University, Chengdu 610039, China
[b] Chongqing Key Laboratory of Speciality Food Co-Built by Sichuan and Chongqing, Chengdu 610039, China
[c] Food Industry Collaborative Innovation Center, Xihua University, Chengdu 610039, China
[d] Chongqing Institute for Food and Drug Control, Chongqing 401121, China
[e] Agricultural Product Processing Institute, Chongqing Academy of Agricultural Science, Chongqing 401329, China
[f] College of Food Science, Southwest University, Chongqing 400715, China

ARTICLE INFO

Keywords:
Capsaicin
Myofibrillar proteins
Interaction mechanisms
Multispectral
Molecular docking
Molecular dynamics simulation

ABSTRACT

The interaction between myofibrillar proteins (MPs) and capsaicin (CAP) was investigated using multispectral, molecular docking, and molecular dynamics simulation methods. The resulting complex increased the hydrophobicity of the tryptophan and tyrosine microenvironment as revealed by fluorescence spectral analysis. The fluorescence burst mechanism study indicated that the fluorescence burst of CAP on the MPs was a static one (Kq $= 1.386 \times 10^{12}$ $m^{-1}s^{-1}$) and that CAP could bind with MPs well (Ka $= 3.31 \times 10^{4}$ L/mol, n $= 1.09$). The analysis of circular dichroism demonstrated that the interaction between CAP and MPs caused a decrease in the α-helical structure of MPs. The complexes formed exhibited lower particle size and higher absolute ζ potential. Furthermore, hydrogen bonding, van der Waals forces, and hydrophobic interactions were found to be the primary factors facilitating the interaction between CAP and MPs, as suggested by molecular docking models and molecular dynamics simulations.

Introduction

As the main compound responsible for the pungent flavor of chili peppers, capsaicin (CAP) plays a critical role in determining their overall spiciness level and quality. CAP has various applications in food and medicine, including as a modulator of metabolism (Lu et al., 2019), antibacterial (Wang, Yu, Zhang, Zhou & Jiang, 2019), pain reliever (Baranidharan, Das & Bhaskar, 2013), antioxidant (Maksimova, Mirceski, Gulaboski, Gudeva & Sarafinovska, 2016), anti-inflammatory (Ghiasi, Esmaeli, Aghajani, Ghazi-Khansari, Faramarzi & Amani, 2019), anticancer (Friedman et al., 2018), and weight loss agent (Lu, Cao, Ho & Huang, 2017). Chili peppers are often liberally added for seasoning while processing Sichuan meat dishes. However, the interactions between muscle protein and CAP, the main pungent component of chili peppers, have been less systematically investigated.

Around 55–60% of the total muscle protein composition is made up of myofibrillar proteins (MPs) (Xia et al., 2019), its physicochemical properties have a notable influence on the quality of meat and meat products. Although MPs have no obvious odor, they can combine with flavor substances, thus improving and regulating the flavor of meat products. Yin, Gao, Wang, Chen and Kong (2022) studied the interaction between furan derivatives and pork MPs and observed that the binding capacity of MPs decreased in the order of 5-methyl furfural > furfural > 2-acetyl furan > furanol. The results indicate that hydrogen bonding, van der Waals forces, and hydrophobic interactions are the main ways that MPs interact with the four furan derivatives. Wang, Zhang, Liu, Xia, Chen and Kong (2022) explored the interactions of pork MPs with 2-pentyl ketone, 2-hexanone, and 2-heptanone through molecular docking and observed that hydrophobic interactions were the main driving force for interactions between MPs and these ketones. Sun et al. (2023) found that hydrophobic interactions and hydrogen bonds between amino acid residues in MPs and flavor compounds from spices can lead to the

* Corresponding authors at: College of Food and Bioengineering, Xihua University, Chengdu 610039, China.
E-mail addresses: wendyjiejie@tom.com (J. Tang), dongzhang@mail.xhu.edu.cn (D. Zhang).

https://doi.org/10.1016/j.fochx.2023.100734
Received 18 April 2023; Received in revised form 22 May 2023; Accepted 31 May 2023
Available online 3 June 2023

formation of stable complexes with CAP. Currently, the interactions between MPs and CAP have been scarcely investigated, and the conformational changes related to the binding of MPs with CAP are poorly understood. Thus, thoroughly studying the molecular mechanism underlying the interactions between CAP and MPs can offer comprehensive guidance for accurately controlling the spicy taste and enhancing the quality of Sichuan meat dishes.

The research employed UV–Vis absorption spectroscopy, simultaneous fluorescence spectroscopy, ζ potential, and circular dichroism (CD) to examine how MPs bind to CAP, including their binding capacity and mode. Furthermore, molecular docking and molecular dynamics simulations were used to identify both the binding sites and types of interactions involved. The findings can offer crucial insights into the interplay between CAP and MPs, and guide the precise regulation of Sichuan meat dishes' spiciness.

Material and methods

Materials

The study used pork tenderloin obtained from a local food supermarket (Pidu, Chengdu), which came from 5-month-old female fragrant pigs. The acid was drained off, and the pH value of fresh pork tenderloin was approximately 6.05. CAP (97%) was purchased from MACKLIN.

Extraction of MPs

MPs were obtained using methods that were reported before (Zhang et al., 2020). Initially, the meat was blended with cooled phosphate-buffered saline (PBS) in a 1:4 ratio. The PBS solution contained 0.1 M NaCl, 1 mM ethylene diamine tetraacetic acid (EDTA), 2 mM $MgCl_2$, had a pH of 7.0, and was kept at 4 °C. The mixture was then homogenized using a homogenizer (FSH-2A, Shanghai Jipad Instrument Co., Ltd, China) for 30 s at intervals of 1 min at a speed of 8,000 rpm. To obtain the precipitate, the homogenate was centrifuged at 8,000 rpm for 15 min at 4 °C. These steps were repeated thrice. Then, four volumes of PBS (0.01 mol/L, 0.1 mol/L NaCl, pH 6.25) were added, homogenized for 30 s at 8,000 rpm, and after 1 min, homogenized again for another 30 s. The precipitate was obtained by centrifugation. These steps were repeated twice. In the end, PBS (pH 6.0) was introduced to the precipitate, mixed for 30 s at a speed of 8,000 rpm, and then passed through gauze via filtration.

Preparation of MPs and CAP solution

First, a CAP stock solution was prepared containing 30% anhydrous ethanol. Afterward, the MPs were thinned to 10 mg/mL concentration by using 20 mM PBS (pH 6.5). To create solutions of MPs with different CAP concentrations, the stock solution and protein solution were mixed in suitable volumes.

UV–Vis absorption spectroscopy

An UV-16001 Shimadzu Corp spectrometer from Kyoto, Japan was utilized to obtain UV–Vis absorption spectra at wavelengths of 235 to 320 nm with adjustments made to the method employed by Shen et al. (2022). In the mixture of CAP and MPs, the concentration of CAP was 0–80 μM, and that of MPs was 0.5 mg/mL.

Fluorescence spectroscopy

A fluorescence spectrophotometer (FLUOROMAX-4cp, HORIBA Jobin Yvon, USA) was employed to measure fluorescence spectra following the method of Kang, Kong, Hu, Li and Ma (2023) with slight modifications. The experiment measured fluorescence using an excitation wavelength of 280 nm and recorded the light spectrum between 280 nm and 475 nm. Synchronous fluorescence spectra were also taken with a 5 nm slit width and scanning speed of 1500 nm/min, with Δλ values of 15 and 60 nm. The sample had a combination of CAP and MPs, with concentrations ranging from 0 to 80 μM for CAP and 0.5 mg/mL for MPs.

Circular dichroism measurements

The method described by Dai et al. (2021) was used to determine the secondary structures of MPs by a circular dichroism spec-trometer (Chirascan V100, Applied Photophysics Limited, UK). CAP was present in the mixed solution at concentrations ranging from 0 to 80 μM, while MPs were present at a concentration of 0.2 mg/mL.

Measurement of particle size and ζ potential

The particle size and ζ potential of MPs were measured using a ZEN3600 particle size potential analyzer from Malvern Instruments Ltd., UK (Pan et al., 2022). The mixture contained MPs at a concentration of 0.5 mg/mL and CAP at concentrations ranging from 0 to 80 μM.

Molecular docking and molecular dynamics simulation

Molecular docking

CAP was bound with myosin using AutoDock vina software package, which followed Liu et al.'s (2023) method but with minor adjustments. The CAP structure (PubChem CID: 1548943) was obtained from the National Library of Medicine (https://www.ncbi.nlm.nih.gov/) through download. The myosin model was obtained from porcine myosin (Q9TV62) by homology modeling. The ligands were first removed from the resulting protein model. Afterwards, AutoDock Tools was used to remove the receptor protein and ligand small-molecule structures from water molecules and add any absent hydrogen atoms to the myosin. To evaluate potential binding sites for CAP and myosin, 50 blind docking sessions were conducted with a grid of size 106 × 126 × 126 along the X, Y, and Z axes. The resulting docking patterns were then analyzed using PyMoL software 2.2.0.

Molecular dynamics simulation

The program GROMACS 2020 was used for molecular dynamics simulations, with minor adjustments to the approach described by Wang et al. (2022). Before the simulation, the protein and ligand were docked using the software AutoDock vina to select the best binding conformation as the initial complex structure for molecular dynamics simulation. The complex small molecules generate topology files in the GAFF force field, and the proteins generate corresponding parameterization files in the AMBER99SB-ILDN force field. Next, a cubic water box was created by adding SPC/E water model molecules to the complex's center. Additionally, three Cl^- ions were incorporated within the water box to maintain the electrical neutrality of the simulated system. The system underwent a 50,000-step energy minimization process using the steepest energy descent method to achieve stability once it was completed. The canonical ensemble (NVT) with the Berendsen heat bath method was used to maintain the temperature at 298.15 K. The simulation consisted of 50,000 steps and each step had a duration of 2 fs. Then, an isothermal isobaric system synthesis (NPT), Parrinello-Rahman pressure control, 1 atmosphere, 50,000 simulation steps, and 2 fs step size were used. The function mdrun was executed using a time step of 2 fs and 15,000,000 simulations, totaling 30 ns of simulations. The data were obtained, analyzed, and mapped accordingly.

Statistical analyses

SPSS 22 was utilized to process experimental data and Tukey's test with a significance level of 5% ($P < 0.05$) was employed to identify significant differences in all statistical analyses.

Results and discussion

UV–Vis absorption spectra.

UV–Vis absorption spectra are useful for characterizing the interactions between small molecules and proteins, or for studying the formation of new complex systems (Han et al., 2022). Fig. 1(a) presents the UV–Vis absorption spectra of MPs at different CAP concentrations (0–80 μM). All spectra showed absorption peaks at 280 nm, suggesting the presence of aromatic amino acids such as tryptophan (Trp), tyrosine (Tyr), and phenylalanine (Phe) (Shen, Huang, Zhao & Sun, 2019). As the CAP concentration increased, the absorbance of the MPs solution gradually rose and exhibited a minor red shift (from 274 to 276 nm). The increase in absorbance of the complex is due to CAP's association with the aromatic amino acids present in MPs, while the shift towards longer wavelengths in maximum absorbance signals a modification in the microenvironment of these residues (Satheshkumar & Elango, 2014). This indicated that the binding of CAP with MPs may alter the latter's structure. Due to the limited sensitivity of the method, the interaction between MPs and CAP was further explored using fluorometric assays.

Fluorescence spectra

In general, the aromatic amino acids (Trp and Tyr) in proteins have absorption peaks at 280 nm excitation wavelength (Sun, Wang, Liu, Kong & Chen, 2021). Trp and Tyr residues are frequently employed to examine protein conformational changes and intermolecular interactions due to their high sensitivity to the surrounding microenvironment, making them important techniques for characterize the tertiary structure of proteins (Lefevre, Fauconneau & Thompson, 2007). As presented in Fig. 1(b). The fluorescence of MPs decreased with an increase in the concentration of CAP, suggesting that the addition of CAP caused the bursting of MPs' fluorescence. Typically, while Trp and Tyr reside within the hydrophobic protein interior, they may also be exposed due to denaturation or ligand binding-induced structural alterations (Wang, Xia, Yin, Liu, Chen & Kong, 2021). The interaction between CAP and MPs modifies the microenvironment around Trp and Tyr residues of myosin. The decrease in fluorescence intensity at 340 nm indicates that this interaction occurs near the hydrophobic region adjacent to these residues.

By analyzing the fluorescence data using the Stern-Volmer equation, the mechanism responsible for the fluorescence burst triggered by CAP was studied (Ying et al., 2018):

$$F_0/F = 1 + K_{SV}[Q] = 1 + K_q\tau_0[Q] \quad (1)$$

F_0 represents the highest fluorescence intensity of MPs that lack CAP, whereas F represents the maximum fluorescence intensity of MPs with different concentrations of CAP. K_{SV} is the fluorescence burst constant of CAP on MPs, expressed in L/mol. [Q] denotes the concentration of CAP in mol/L. K_q, expressed in L/mol·s, is the rate constant for bimolecular quenching, and τ_0 is the fluorophore's lifetime without a quencher, which is 10^{-8} s.

The fluorescence burst mechanism was divided into dynamic burst and static burst (Yao, Xu, Zhang, Zheng, Liu & Zhang, 2021). The highest value for the scattering collisional burst constant of different bursting agents with biopolymers was 2.0×10^{10} $m^{-1}s^{-1}$ (Wang et al., 2022), in the context of dynamic bursting. The linear relationship between the F_0/F and [Q] curves is presented in Fig. 2(a), and the burst constant K_q calculated from the experimental data was 1.386×10^{12} $m^{-1}s^{-1}$. The results obtained were much higher than 2.0×10^{10} $m^{-1}s^{-1}$, which proved that the burst mechanism of CAP on MPs was not caused by a dynamic burst but due to the static burst of CAP combined with MPs.

The provided formula can be utilized for determining the binding constants and the quantity of binding sites (static burst):

$$\log[(F_0 - F)/F] = \log K_a + n \log[Q] \quad (2)$$

The values for F_0, F, and [Q] are consistent with those obtained from the Stern-Volmer equation. The binding constant is denoted as K_a and the number of binding sites as n. The intercept and slope of the log(F_0-F)/F versus log [Q] plot determine the K_a and n values for the CAP and MPs complexes. A strong binding effect between CAP and the MPs is suggested by the K_a value of 3.31×10^4 L/mol and n of 1.09 that was determined (Fig. 2(b)).

Synchronous fluorescence spectroscopy

The emission wavelength shift of fluorescent groups, such as Tyr and Trp residues, can be used to monitor the microenvironment of amino acid residues (Yin, Gao, Wang, Chen & Kong, 2022). Fluorescence spectra, which reveal information about the properties of Tyr and Trp residues, were obtained simultaneously by setting the excitation and emission wavelengths to 15 nm and 60 nm, respectively. This is illustrated in Fig. 3(a) and (b). As the concentration of CAP increased, the fluorescence intensity of Trp and Tyr residues decreased in MPs, and there was a slight blue shift in the maximum absorption peak (4 nm). This indicates that the interaction between CAP and MPs altered the microenvironment of both residues, leading to a decrease in the polarity of the adjacent environment and an increase in hydrophobicity near the amino acid residues (Yu et al., 2020). Trp residues have greater fluorescence intensity than Tyr residues, suggesting they contribute more to

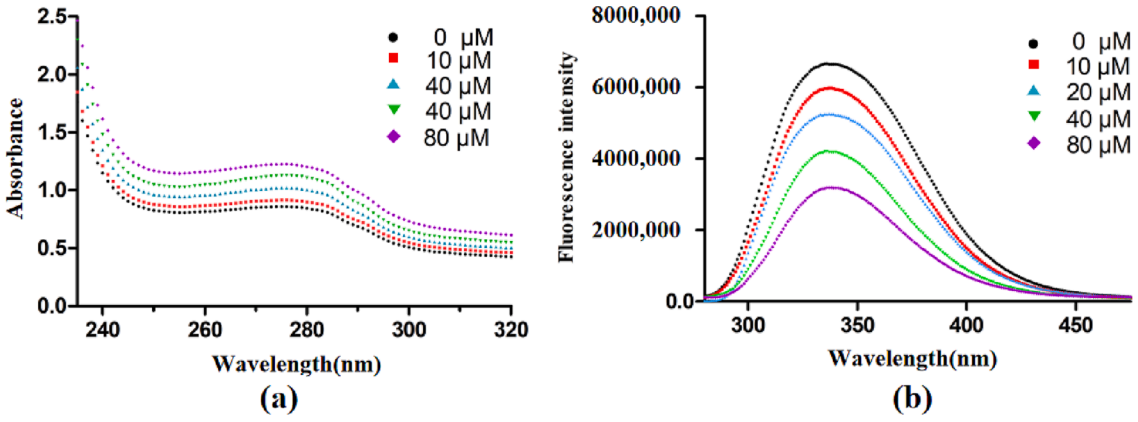

Fig. 1. The effect of different capsaicin concentrations on the UV–Vis spectroscopy (a) and fluorescence emission spectra at 280 nm excitation wavelength (b) of MPs. Notes: ● (black) represents MPs without added capsaicin; ■ (Red) represents MPs with added 10 μM capsaicin; ▲ (Blue) represents MPs with added 20 μM capsaicin; ▼ (Green) represents MPs with added 40 μM capsaicin; ◆ (Purple) represents MPs with added 80 μM capsaicin. (For interpretation of the references to colour in this figure legend, the reader is referred to the web version of this article.)

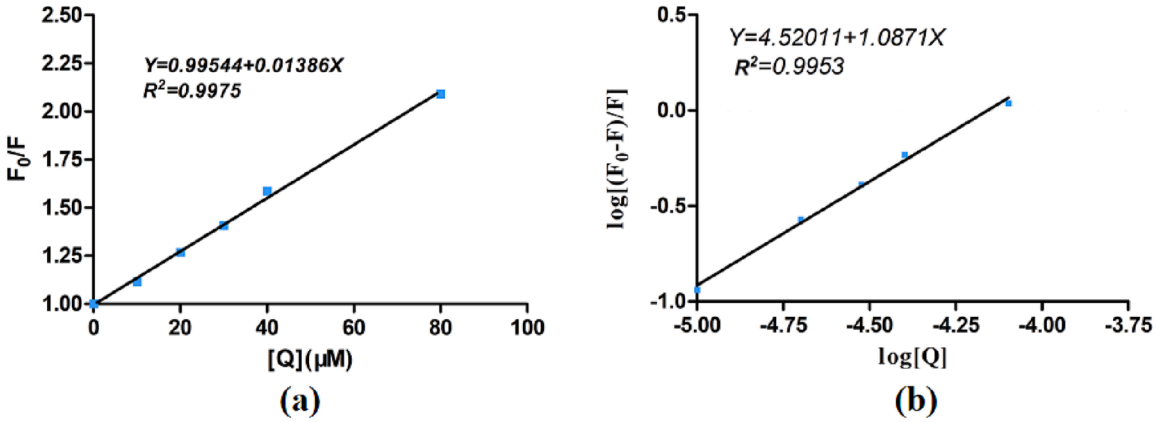

Fig. 2. Stern-Volmer curve of capsaicin-induced fluorescence quenching (a) and logarithmic plot of capsaicin-induced fluorescence quenching (b) in MPs.

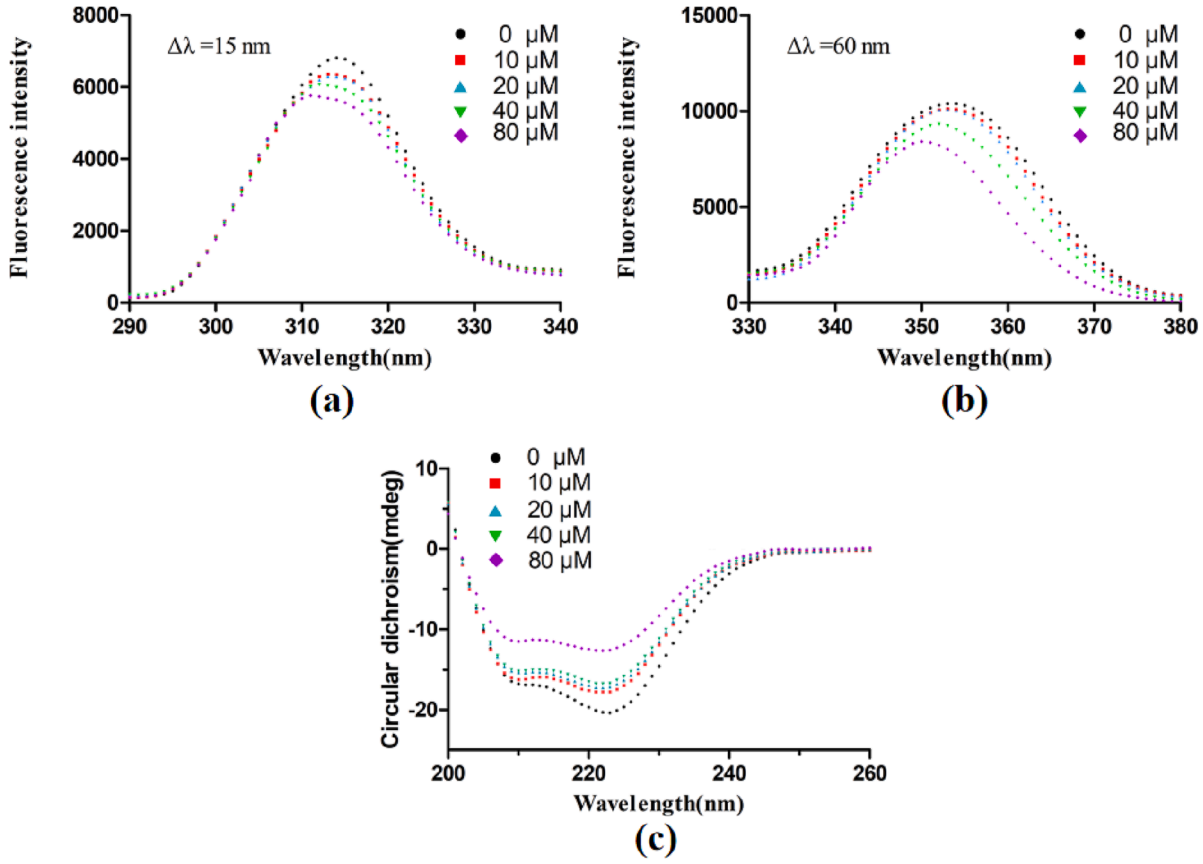

Fig. 3. Effect of different concentrations of capsaicin on the synchronous fluorescence spectrum (Δλ = 15 nm) (a), synchronous fluorescence spectrum (Δλ = 60 nm) (b) and Far-UV CD spectra (c) of MPs. Notes: ● (black) represents MPs without added capsaicin; ■ (Red) represents MPs with added 10 μM capsaicin; ▲ (Blue) represents MPs with added 20 μM capsaicin; ▼ (Green) represents MPs with added 40 μM capsaicin; ◆ (Purple) represents MPs with added 80 μM capsaicin. (For interpretation of the references to colour in this figure legend, the reader is referred to the web version of this article.)

MPs' intrinsic fluorescence (Wang, Ye, Zhao & Yu, 2008). This indicates that the interaction site between CAP and MPs may be near Trp and Tyr amino acids, CAP might induce structural changes in MPs by binding to these residues.

Circular dichroism measurements

The change of protein conformation can be characterized by CD spectrum (Zhang et al., 2022). Fig. 3(c) shows that in the absence of CAP, two negative bands at 212 and 221 nm were detected, indicating the presence of α-helical structure in proteins. This is the primary type of secondary structure found in proteins (Zhang et al., 2021). With an increase in CAP concentration, the intensity of the negative band decreased gradually, suggesting a loss of the α-helical structure. Thus, there was an interaction between CAP and MPs, which increased with increasing CAP content. Hydrogen bonding between the amide C—O and N—H groups is the primary stabilizing factor for the α-helical structure (Wang, He, Gan & Li, 2018). However, the interaction between CAP and MPs weakens internal hydrogen bonds while strengthening external ones, leading to a decrease in the α-helical structure. This concept was verified through molecular docking and dynamic simulations.

Particle size and ζ potential

The particle size of MPs at pH 6.5 was 1155 nm, whereas that of the complexes bound with different concentrations of CAP decreased significantly to 1060.33, 953.67, 886.13, and 854.53 nm, respectively (Table S1). The relatively small particle sizes of the complexes after the addition of CAP compared to the unbound MPs may be because the addition of CAP promoted the noncovalent interactions with proteins, inhibited the aggregation caused by protein–protein interactions, and converted the larger aggregated particles of the complexes into smaller aggregated particles. This result agrees with the findings of Zhan et al. (2020) who confirmed that interactions between CAP and β-lactoglobulin lead to a reduction in protein particle size.

The natural MPs carried a negative charge, and as the concentration of CAP increased, the absolute ζ potential of the fibronectin complexes formed with CAP-MPs also increased (Table S1). The reason for this could be the interplay between CAP and MPs, which causes modifications in the structure of MPs, exposes the protein's negative charge, and ultimately changes the ζ potential. It is suggested that the addition of CAP promotes its interaction with MPs and maintains a stable complex structure by forming hydrogen bonds, while the higher absolute ζ potential generates electric repulsion that prevents particle aggregation, resulting in smaller particle sizes (Sui, Sun, Qi, Zhang, Li & Jiang, 2018).

Molecular docking

Myosin is the major protein in MPs (Zhang et al., 2020). Myosin was selected as the receptor to bind with CAP. A homology model was generated using myosin's amino acid sequence (UniProtKB-Q9TV62) and 96.14% of its amino acids were correctly positioned, as indicated by the Ramachandran plot (Fig. 4(a)).

Molecular docking is a technique that can identify how small molecules and receptors bind together, as well as their strength of interaction (Wu, Xiao, Yue, Zhong, Zhao & Gao, 2020). In the docking state, CAP was found to have formed a stable complex with myosin, as shown by the molecular docking results (Fig. 4(b)), with a selected binding free energy of −4.86 KJ/mol. As shown in Fig. 5(a) and 5(b), hydrophobic interaction exist between residues Ala-429, Asp-598, and Pro-603 of myosin and CAP, while CAP forms hydrogen bonds with bond lengths of 2.3 and 2.0 Å through residues Lys-432 and Lys-599, respectively. These results align with the findings from CD, which demonstrated that the stability of the complexes depends on hydrogen bonding and hydrophobic interactions between the protein and small-molecule ligand CAP. These interactions play a crucial role in maintaining the complexes' 3D structural stability. Moreover, Asp-598, Asp-602, Ala-429, Cys-480, Glu-272, Lys-273, Leu-270, Leu-271, Leu-476, Ser-274, and Val-649 in myosin interact with myosin through van der Waals forces (Fig. 5(c)).

Molecular dynamics simulation

Root mean square fluctuations (RMSF)

During the simulation, the RMSF method was used to measure the average movement of atomic positions in the molecular structure over a period and represented the root mean square of the distance of a structure-specific atom concerning the reference structure over the entire time range, characterizing the flexibility of the protein, with higher fluctuations in the RMSF representing higher flexibility of the amino acid and leading to unstable binding (Yu et al., 2021). CAP binding restricted myosin fluctuations, leading to lower fluctuations in the complex during the simulation period (Fig. 6(a)). Consequently, the complex was more structurally stable than myosin. Significant changes in amino acid RMSF values were observed in the regions located at 202–214, 631–643, and 787–808, indicating that these positions were the sites of interaction for the CAP-protein complexes. Therefore, the conformation of the protein was changed by the interactions between CAP and myosin.

Radius of gyration (Rg)

The Rg determines the structural activity by estimating the distribution of atoms around the protein axis (Sneha & George Priya Doss, 2016) and is used to measure the tightness or degree of folding of the molecular structure. Throughout the simulation, the Rg values of the complexes were consistently lower than those of myosin. This implies that the complexes have become more dense and their internal interactions have been strengthened, possibly due to decreased moments. At 20 ns of simulation, Rg reached a constant value, indicating that the molecular dynamics simulation reached equilibrium after 20 ns. Upon reaching equilibrium, the Rg value of the complex was notably decreased compared to myosin alone, indicating that the binding of CAP with myosin led to significant structural changes, resulting in a denser protein structure (Fig. 6(b)).

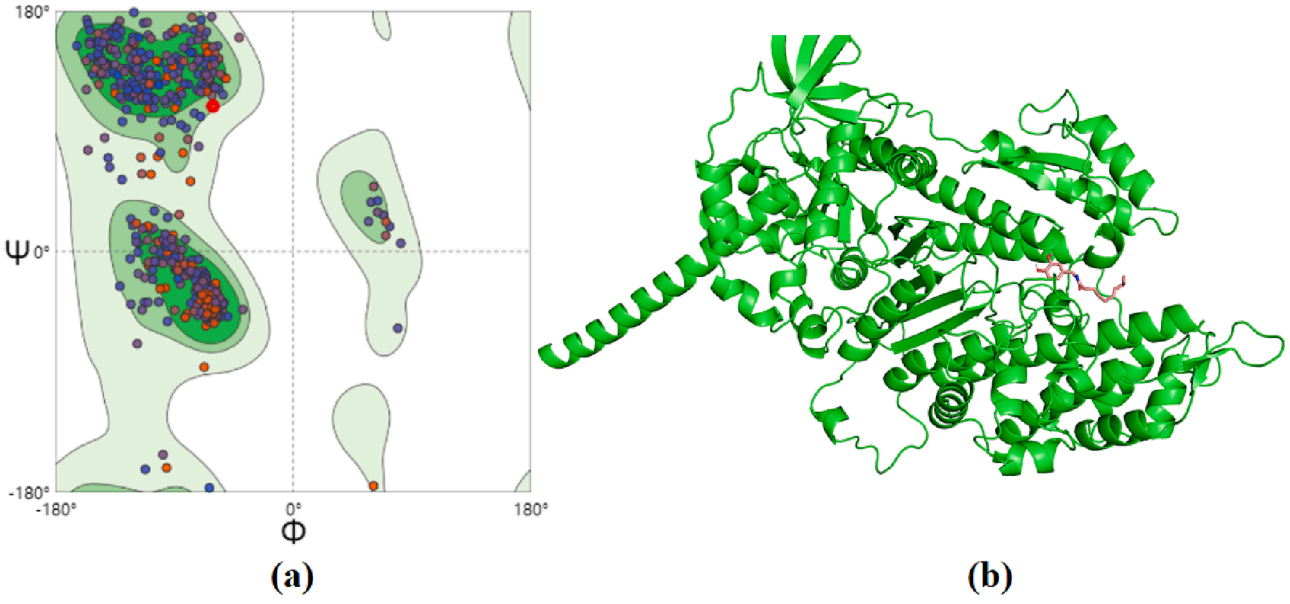

Fig. 4. Ramachandran plot for the homology model (a), and molecular docking model (3D) (b) of myosin and capsaicin.

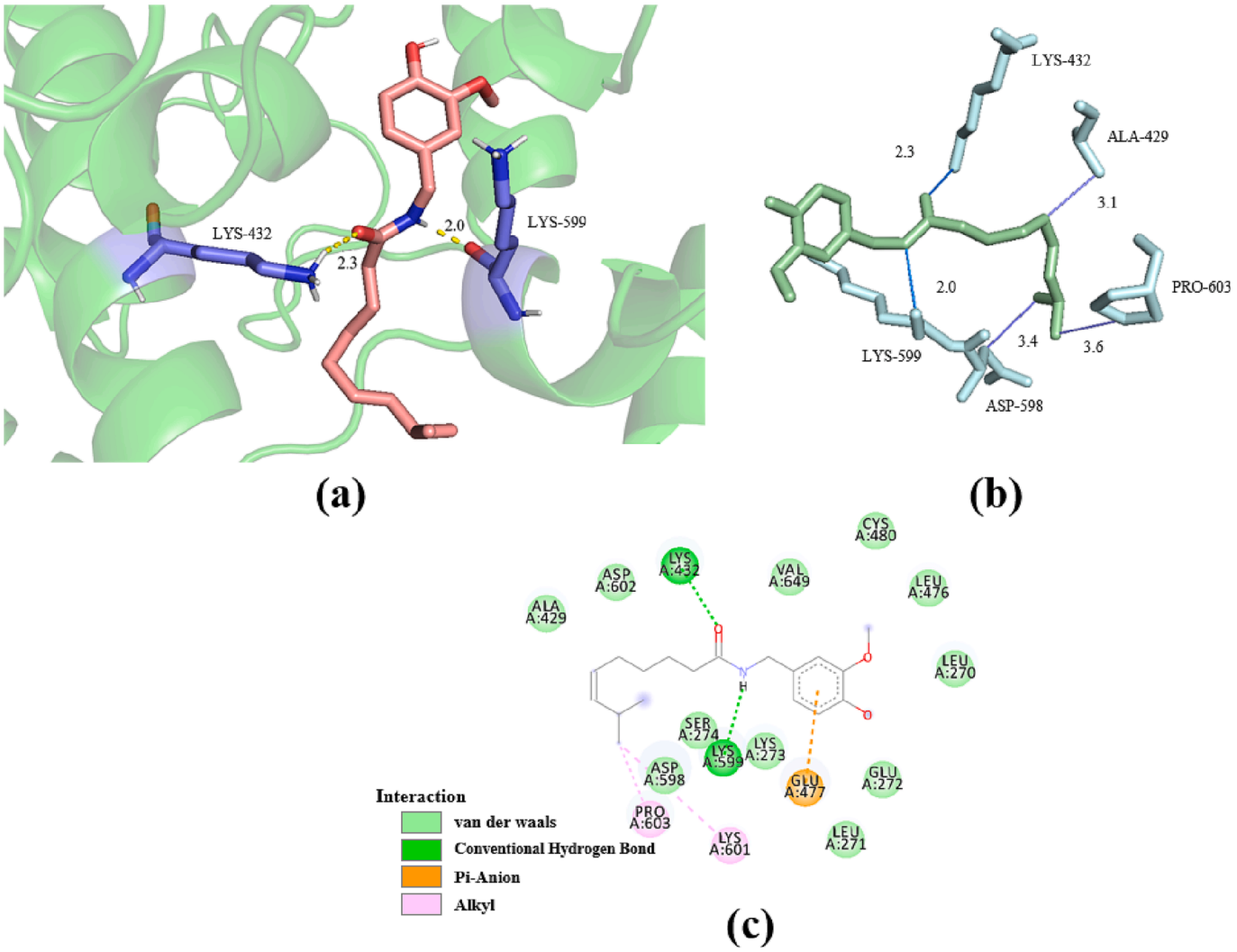

Fig. 5. Hydrogen bonds formed by capsaicin with Lys-432 and Lys-599 in myosin (2.3 Å and 2.0 Å) (a), hydrogen bond and hydrophobic interaction between capsaicin and myosin (b), and molecular docking model (2D) of myosin and capsaicin (c). Notes: (yellow) represents hydrogen bond, the stick models represent capsaicin and key amino acid residues; (blue) represents hydrogen bond; (purple) represents hydrophobic interaction. (For interpretation of the references to colour in this figure legend, the reader is referred to the web version of this article.)

Molecular Mechanics/Poisson-Boltzmann surface area (MMPBSA)

The MMPBSA method computes the disparity in binding free energy between two solvent-containing molecules when they are in their bound and unbound forms. The calculation of the MMPBSA for the complex was performed using a specific formula:

$$\Delta G_{bind} = \Delta E_{vdw} + \Delta E_{cou} + (\Delta G_{polar} + \Delta G_{non\ -\ polar}) \quad (3)$$

Where ΔE_{vdw} represents van der Waals interaction energy, ΔE_{cou} represents intermolecular electrostatic binding energy, ΔG_{polar} is the polarized solvent-free energy, $\Delta G_{non\text{-}polar}$ is the nonpolarized solvent-free energy. The interactions between proteins and small-molecule compounds were evaluated by calculating the binding free energy (Farhadian, Shareghi, Asgharzadeh, Rajabi & Asadi, 2019). The calculation in Fig. S1 used the final 10 ns of the equilibrium state trajectory. The binding energy between small molecules and proteins was determined to be −149.433 KJ/mol, indicating that they can bind strongly and spontaneously. Van der Waals interaction energy (−240.538 KJ/mol), intermolecular electrostatic binding energy (−16.541 KJ/mol), polarized solvent-free energy (122.350 KJ/mol), and nonpolarized solvent-free energy (−25.542 KJ/mol) are the forces that dominate the interactions between myosin and CAP.

Conclusion

In short, the results of UV–Vis absorption spectra indicated that CAP formed complexes with MPs. According to the fluorescence data, CAP's interaction with MPs changes the microenvironment of Trp and Tyr and binds to the hydrophobic regions close to these moieties. Moreover, CAP bursts the fluorescence of MPs by static burst (Kq = 1.386×10^{12} $m^{-1}s^{-1}$). The CD measurements showed that MPs' conformation changed and the α-helical structure decreased when binding to CAP. The results of molecular docking and dynamics simulations showed that CAP could bind with myosin with a low binding free energy (−4.86 KJ/mol), wherein myosin formed hydrogen bonds with CAP via Lys-432 and Lys-599, while Ala-429, Asp-598, and Pro-603 formed hydrophobic bonds with CAP. Both types of bonds promoted the formation of the complexes and ensured their stability. This study reveals the interaction mechanism between CAP and MPs, which provides more adequate theoretical support for precise regulation of the spicy flavor and improvement of the quality characteristics of Sichuan meat dishes.

Data availability statement

All data supporting the findings of this study are available in the

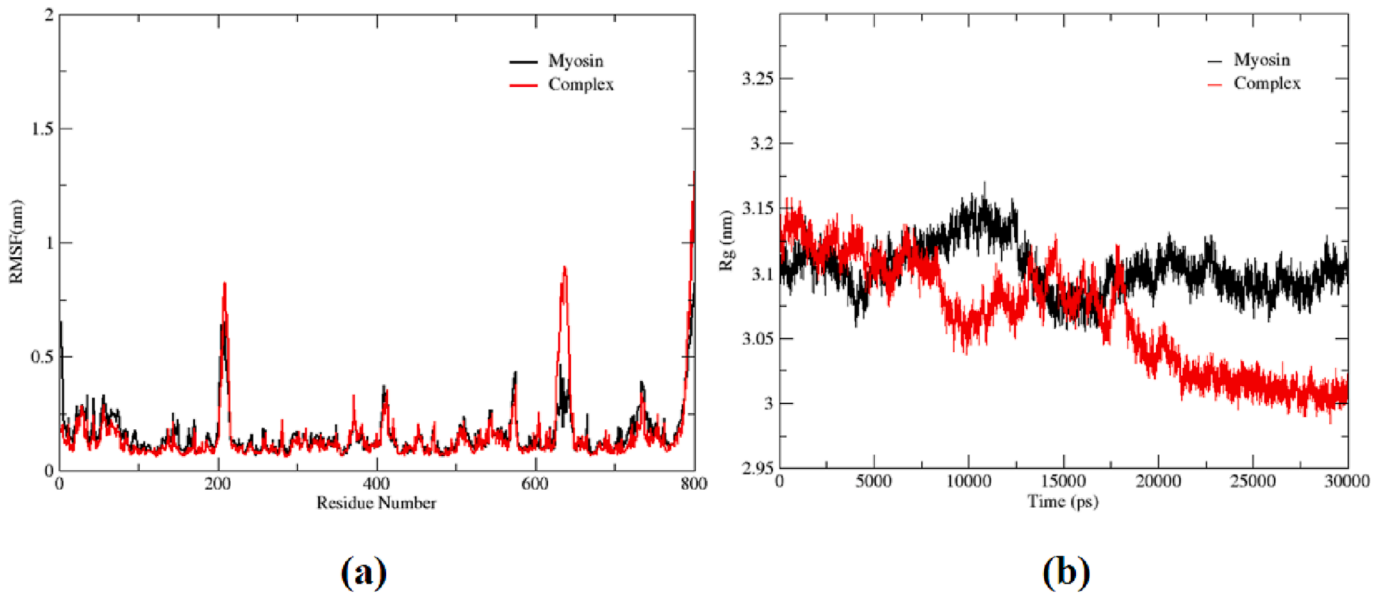

Fig. 6. Analysis of root mean square deviation (RMSD) (a) and analysis of radius of gyration (Rg) (b). Notes: ▬ (black) represents individual myosin; ▬ (red) represents complexes of myosin and capsaicin. (For interpretation of the references to colour in this figure legend, the reader is referred to the web version of this article.)

article or upon request from the corresponding author.

CRediT authorship contribution statement

Zhicheng Wu: Methodology, Investigation, Writing – review & editing. **Jingbing Xu:** Investigation. **Jinggang Ruan:** Investigation. **Jiaxin Chen:** Methodology. **Xue Li:** Investigation. **Yiru Yu:** Investigation. **Xinrui Xie:** Investigation. **Jie Tang:** Conceptualization, Supervision, Funding acquisition. **Dong Zhang:** Formal analysis, Conceptualization, Supervision, Funding acquisition. **Hongjun Li:** Formal analysis.

Declaration of Competing Interest

The authors declare that they have no known competing financial interests or personal relationships that could have appeared to influence the work reported in this paper.

Data availability

The data that has been used is confidential.

Acknowledgements

This research was funded by Science and Technology Department of Sichuan Province, China (23ZDYF3100), Natural Science Foundation of Sichuan Province, China (2022NSFSC1758), Chengdu Science and Technology Bureau, Sichuan Province, China (2022-YF09-00018-SN), Xihua University Talent Introduction Project (Z211046), and Chongqing Municipal Technology Innovation and Application Development Special Key Project (grant number cstc2021jscx-cy1hX0014).

Appendix A. Supplementary data

Supplementary data to this article can be found online at https://doi.org/10.1016/j.fochx.2023.100734.

References

Baranidharan, G., Das, S., & Bhaskar, A. (2013). A review of the high-concentration capsaicin patch and experience in its use in the management of neuropathic pain. *Therapeutic Advances in Neurological Disorders, 6*(5), 287–297.

Dai, H., Sun, Y., Xia, W., Ma, L., Li, L., Wang, Q., & Zhang, Y. (2021). Effect of phospholipids on the physicochemical properties of myofibrillar proteins solution mediated by NaCl concentration. *LWT-Food Science and Technology, 141*, Article 110895.

Farhadian, S., Shareghi, B., Asgharzadeh, S., Rajabi, M., & Asadi, H. (2019). Structural characterization of α-chymotrypsin after binding to curcumin: Spectroscopic and computational analysis of their binding mechanism. *Journal of Molecular Liquids, 289*, Article 111111.

Friedman, J. R., Nolan, N. A., Brown, K. C., Miles, S. L., Akers, A. T., Colclough, K. W., … Dasgupta, P. (2018). Anticancer activity of natural and synthetic capsaicin analogs. *Journal of Pharmacology and Experimental Therapeutics, 364*(3), 462–473.

Ghiasi, Z., Esmaeli, F., Aghajani, M., Ghazi-Khansari, M., Faramarzi, M., & Amani, A. (2019). Enhancing analgesic and anti-inflammatory effects of capsaicin when loaded into olive oil nanoemulsion: An in vivo study. *International Journal of Pharmaceutics, 559*, 341–347.

Han, P., An, N., Yang, L., Ren, X., Lu, S., Ji, H., … Dong, J. (2022). Molecular dynamics simulation of the interactions between sesamol and myosin combined with spectroscopy and molecular docking studies. *Food Hydrocolloids, 131*, Article 107801.

Kang, Z., Kong, L., Hu, Z., Li, Y., & Ma, H. (2023). Effect of sodium bicarbonate and sodium chloride on protein conformation and gel properties of pork myofibrillar protein. *Arabian Journal of Chemistry, 16*, Article 104574.

Lefevre, F., Fauconneau, B., Thompson, J. W., & Gill, T. A. (2007). Thermal denaturation and aggregation properties of Atlantic salmon myofibrils and myosin from white and red muscles. *Food Chemistry, 55*(12), 4761–4770.

Lu, M., Cao, Y., Ho, C., & Huang, Q. (2017). The enhanced anti-obesity effect and reduced gastric mucosa irritation of capsaicin-loaded nanoemulsions. *Food & Function, 8*(5), 1803–1809.

Lu, M., Lan, Y., Xiao, J., Song, M., Chen, C., Liang, C., … Ho, C. (2019). Capsaicin ameliorates the redox imbalance and glucose metabolism disorder in an insulin-resistance model via circadian clock-related mechanisms. *Journal of Agricultural and Food Chemistry, 67*(36), 10089–10096.

Liu, Y., Mubango, E., Dou, P., Bao, Y., Tan, Y., Luo, Y., … Hong, H. (2023). Insight into the protein oxidation impact on the surface properties of myofibrillar proteins from bighead carp. *Food Chemistry, 411*, Article 135515.

Maksimova, V., Mirceski, V., Gulaboski, R., Gudeva, L. K., & Sarafinovska, Z. A. (2016). Electrochemical evaluation of the synergistic effect of the antioxidant activity of capsaicin and other bioactive compounds in capsicum sp. extracts. *International Journal of Electrochemical Science, 11*, 6673–6687.

Pan, N., Wan, W., Du, X., Kong, B., Liu, Q., Lv, H., … Li, F. (2022). Mechanisms of change in emulsifying capacity induced by protein denaturation and aggregation in quick-frozen pork patties with different fat levels and freeze–thaw cycles. *Foods, 11*(1), 44.

Satheshkumar, A., & Elango, K. P. (2014). Spectroscopic and molecular docking studies on the charge transfer complex of bovine serum albumin with quinone in aqueous medium and its influence on the ligand binding property of the protein. *Spectrochimica Acta Part A: Molecular and Biomolecular Spectroscopy, 130*, 337–343.

Shen, H., Huang, M., Zhao, M., & Sun, W. (2019). Interactions of selected ketone flavours with porcine myofibrillar proteins: The role of molecular structure of flavour compounds. *Food Chemistry, 298*, Article 125060.

Shen, S., Bu, Q., Yu, W., Chen, Y., Liu, F., Ding, Z., & Mao, J. (2022). Interaction and binding mechanism of lipid oxidation products to sturgeon myofibrillar protein in low temperature vacuum heating conditions: Multispectroscopic and molecular docking approaches. *Food Chemistry, 15*, Article 100389.

Sneha, P., & George Priya Doss, C. (2016). Molecular dynamics: New frontier in personalized medicine. *Advances in Protein Chemistry and Structural Biology, 102*, 181–224.

Sui, X., Sun, H., Qi, B., Zhang, M., Li, Y., & Jiang, L. (2018). Functional and conformational changes to soy proteins accompanying anthocyanins: Focus on covalent and non-covalent interactions. *Food Chemistry, 245*, 871–878.

Sun, F., Wang, H., Liu, Q., Kong, B., & Chen, Q. (2021). Effects of temperature and pH on the structure of a protease from Lactobacillus brevis R4 isolated from Harbin dry sausage and molecular docking of the protease to the meat proteins. *Food Bioscience, 42*, Article 101099.

Sun, X., Yu, Y., Saleh, A. S. M., Yang, X., Ma, J., Li, W., … Wang, Z. (2023). Understanding interactions among flavor compounds from spices and myofibrillar proteins by multi-spectroscopy and molecular docking simulation. *International Journal of Biological Macromolecules, 229*, 188–198.

Wang, H., Xia, X., Yin, X., Liu, H., Chen, Q., & Kong, B. (2021). Investigation of molecular mechanisms of interaction between myofibrillar proteins and 1-heptanol by multiple spectroscopy and molecular docking methods. *International Journal of Biological Macromolecules, 193*, 672–680.

Wang, H., Zhang, H., Liu, Q., Xia, X., Chen, Q., & Kong, B. (2022). Exploration of interaction between porcine myofibrillar proteins and selected ketones by GC–MS, multiple spectroscopy, and molecular docking approaches. *Food Research International, 160*, Article 111624.

Wang, N., Ye, L., Zhao, B. Q., & Yu, J. X. (2008). Spectroscopic studies on the interaction of efonidipine with bovine serum albumin. *Brazilian Journal of Medical and Biological Research, 41*(7), 589–595.

Wang, Q., Tang, Y., Yang, Y., Lei, L., Lei, X., Zhao, J., … Ming, J. (2022). Interactions and structural properties of zein/ferulic acid: The effect of calcium chloride. *Food Chemistry, 373*, Article 131489.

Wang, X., Yu, L., Li, F., Zhang, G., Zhou, W., & Jiang, X. (2019). Synthesis of amide derivatives containing capsaicin and their antioxidant and antibacterial activities. *Journal of Food Biochemistry, 43*(12), 13061.

Wang, Z., He, Z., Gan, X., & Li, H. (2018). Effect of peroxyl radicals on the structure and gel properties of isolated rabbit meat myofibrillar proteins. *International Journal of Food Science & Technology, 53*(12), 2687–2696.

Wu, Y., Xiao, Y., Yue, Y., Zhong, K., Zhao, Y., & Gao, H. (2020). A deep insight into mechanism for inclusion of 2R,3R-dihydromyricetin with cyclodextrins and the effect of complexation on antioxidant and lipid-lowering activities. *Food Hydrocolloids, 103*, Article 105718.

Xia, M., Chen, Y., Guo, J., Huang, H., Wang, L., Wu, W., … Sun, W. (2019). Water distribution and textual properties of heat-induced pork myofibrillar protein gel as affected by sarcoplasmic protein. *LWT-Food Science and Technology, 103*, 308–315.

Yao, L., Xu, J., Zhang, L., Zheng, T., Liu, L., & Zhang, L. (2021). Physicochemical stability-increasing effects of anthocyanin via a co-assembly approach with an amphiphilic peptide. *Food Chemistry, 362*, Article 130101.

Ying, M., Meti, M. D., Xu, H., Wang, Y., Lin, J., Wu, Z., … Hu, Z. (2018). Binding mechanism of lipase to Ligupurpuroside B extracted from Ku-Ding tea as studied by multi-spectroscopic and molecular docking methods. *International Journal of Biological Macromolecules, 120*, 1345–1352.

Yin, X., Gao, M., Wang, H., Chen, Q., & Kong, B. (2022). Probing the interaction between selected furan derivatives and porcine myofibrillar proteins by spectroscopic and molecular docking approaches. *Food Chemistry, 397*, Article 133776.

Yu, X., Cai, X., Luo, L., Wang, J., Ma, M., Wang, M., & Zeng, L. (2020). Influence of tea polyphenol and bovine serum albumin on tea cream formation by multiple spectroscopy methods and molecular docking. *Food Chemistry, 333*, Article 127432.

Yu, Z., Kan, R., Ji, H., Wu, S., Zhao, W., Shuian, D., … Li, J. (2021). Identification of tuna protein-derived peptides as potent SARS-CoV-2 inhibitors via molecular docking and molecular dynamic simulation. *Food Chemistry, 342*, Article 128366.

Zhang, D., Li, H., Emara, A. M., Hu, Y., Wang, Z., Wang, M., & He, Z. (2020). Effect of in vitro oxidation on the water retention mechanism of myofibrillar proteins gel from pork muscles. *Food Chemistry, 315*, Article 126226.

Zhang, D., Wu, Z., Ruan, J., Wang, Y., Li, X., Xu, M., … Li, H. (2022). Effects of lysine and arginine addition combined with high-pressure microfluidization treatment on the structure, solubility, and stability of pork myofibrillar proteins. *LWT-Food Science and Technology, 172*, Article 114190.

Zhan, F., Ding, S., Xie, W., Zhu, X., Hu, J., Gao, J., … Chen, Y. (2020). Towards understanding the interaction of β-lactoglobulin with capsaicin: Multi-spectroscopic, thermodynamic, molecular docking and molecular dynamics simulation approaches. *Food Hydrocolloids, 105*, Article 105767.

Zhang, L., Wang, P., Yang, Z., Du, F., Li, Z., Wu, C., … Zhou, G. (2020). Molecular dynamics simulation exploration of the interaction between curcumin and myosin combined with the results of spectroscopy techniques. *Food Hydrocolloids, 101*, Article 105455.

Zhang, Y., Lu, Y., Yang, Y., Li, S., Wang, C., Wang, C., & Zhang, T. (2021). Comparison of non-covalent binding interactions between three whey proteins and chlorogenic acid: Spectroscopic analysis and molecular docking. *Food Bioscience, 41*, Article 101035.